Parallelized 3D optical flow method for fluid mechanics applications

Tamas Regert, Benoit Tremblais, Laurent David

Parallelized 3D optical flow method for fluid mechanics applications

Tamas Regert, Benoit Tremblais
Institut XLIM UMR CNRS 6172
Bât. SP2MI - BP 30179
86962 FUTUROSCOPE CHASSENEUIL Cedex, France.
{regert,tremblais}@sic.univ-poitiers.fr

Laurent David
LEA UMR CNRS 6609
Boulevard Marie et Pierre Curie - BP 30179
86962 FUTUROSCOPE CHASSENEUIL Cedex, France.
laurent.david@univ-poitiers.fr

Abstract

In this paper we address the problem of estimating the motion of fluids in 3D image sequences. We present a 3D extension of the second order div-curl regularization 2D optical flow equation first introduced by Corpetti et al. *In addition, we propose a multigrid and Message Passing Interface (MPI) parallelized implementation of the algorithm to handle the huge amount of data encountered in our applications. The performance of the resulting fluid flow estimator is demonstrated on a well representative motion synthetic pattern called Hill's spherical vortex. The suggested method should be a good alternative or complement to the well established techniques based on 3D cross correlation.*

1. Introduction

In the area of fluid mechanics, the majority of flows which have significant interests for academic research and are representative of industrial situations, reveals the existence of unsteady three-dimensional flow structures. Even if numerical modelling has done substantial progress in fluid mechanics during the last two decades, experimental approaches of these complex phenomena remain essential to understand the physics of the mechanisms of fluid motion and to investigate the industrial problems. In the early 1985's, the advent of two-dimensional optical diagnostics such as Particle Image Velocimetry (PIV) has given access to instantaneous velocity measurements in a slice of the flow [1]. That new flow visualization has significantly modified our description of turbulent flows and in particular has clearly shown the essential role of unsteady structures in the organization of turbulence. It is now established that PIV measurement has a great interest and is considered as a mature optical diagnostic tool for fluid mechanics research. The next challenging issue in the development of optical diagnostics concerns the instantaneous three-dimensional velocity measurements. Very recently, novel approaches based on photogrammetric technique, called tomographic PIV, have been proposed [10, 11]. As a result of this technique the deep details of the flow of fluids become accessible to the researchers, that exhibit a significant contribution in understanding the physics of fluid motion. There are two basic ideas in the corresponding literature concerning the tomographic PIV technique. Each of them uses the same principle of introducing tracer particles that can follow the motion of fluid and of highlighting the flow with a laser. The first idea is to illuminate a portion of the volume of interest by a large laser-sheet and multiple cameras are recording the particles position from different views (cf. Figure. 1). This method leads to an ill posed determination of the location of particles, i.e. one particle can be determined at ambiguous locations. These ambiguous particles are usually referred to as 'ghost particles' and their motion is not consistent with the motion of the fluid [10]. The other idea is the scanning of the volume by a fast moving thin laser sheet. In this case only one camera is recording the position of the particles [11]. The location of particles is in this case correct and non-ambiguous. It should be noted, that the resolution of the cameras is high and should increase in the future. Then, at each time t, each set of projected images is provided to a tomography algorithm to reconstruct a volume of particles. The size of the obtained volume is approximately today $2000 \times 1440 \times 160$ voxels. Finally, from

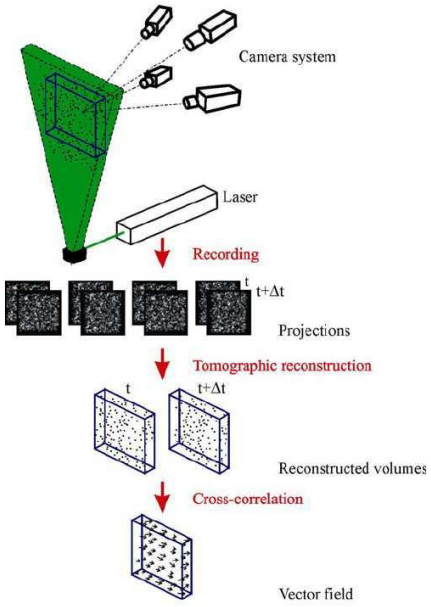

Figure 1. Tomography PIV principle.

two consecutive reconstructed volumes a three-dimensional correlation technique is used to extract the 3D velocity vector field.

In this work the purpose is to determine the displacement field from a sequence of three-dimensional images originating from tomographic PIV experiments and representing the motion of fluid, by means of the optical flow method. The most extensively applied principle for the determination of the field of the displacement vectors in PIV is the conservation of the gray level I of the moving objects in the images during motion. The two basic formulations of the conservation of the gray level are the method of correlation [1] which is its integral formulation, and the optical flow method, also called as Optical Flow Constraint (OFC) [13], which is its differential formulation. One major difference between the integral and the differential formulation is that the integral formulation leads to a so called region-based solution, where each displacement vector belongs to a certain sub-region of the total domain, while the differential formulation provides a possibility for obtaining a vector for the smallest entity of the domain, practically for each pixel/voxel of an image/volume-image. In this paper the differential formulation of the gray level conservation, i.e. the optical flow method is discussed and used. The optical flow method is based on a scalar differential equation (Eq.(1)) and contains the optical flow velocity vector, which is defined in three-dimensional space as $\mathbf{u} = [u\ v\ w]$.

$$\nabla I \cdot \mathbf{u} + I_t = 0, \tag{1}$$

where the subscript indicates partial differentiation in terms of the variable indicated in the subscript, ∇ indicates the gradient operator, t denotes time. This equation is essentially ill posed for determining vector quantities and this disadvantageous character is usually referred to as the aperture problem [13],[3], [5]. To overcome this ill posed character of the optical flow constraint, additional assumptions are needed. The basic ways of making the OFC well posed are:

1. assumption of integrity of motion in a close vicinity of the current location [3], [5] ;
2. assumption of smoothness of some order of derivatives of the displacement field [13];
3. utilization of some governing equations that describe the displacement field theoretically [17], [16], [4]

Similarly to the correlation method, the assumption 1 provides also a region based approach, because a region is needed to compute the local value of displacement. The most popular optical flow method that is based on this assumption is the method of Lucas and Kanade [3]. The other two assumptions are local and no sub-region is needed for the computation. The proposal of [13] belongs to the group indicated by the assumption 2 above. The basic principle to add the so called regularization term to the OFC and form an error functional E that can be minimized by using an appropriate penalty function. In our code quadratic penalty function as well, as robust functions were implemented. The robust functions were formulated according to the proposal of Corpetti et al. [7] and in [5] that leads to a simply implementable algorithm. In the following the equations are demonstrated by using the quadratic penalty function for the sake of simplicity. For a two-dimensional case, using quadratic penalty function, the first order regularization has the form as shown in Eq.(2)).

$$E = \int_{\Omega} \left[\left(\nabla I \cdot \mathbf{u} + I_t \right)^2 + \alpha^2 \cdot \left(|\nabla u|^2 + |\nabla v|^2 \right) \right] d\mathbf{x}, \tag{2}$$

where Ω denotes the domain of the image, α indicates the relative importance of the regularization term over the observation term. The first order regularization leads to the 'penalization' of the derivatives of the optical flow velocity field as a side-effect of making the Eq.(1) well posed. This proposal was refined by [19] to change the first derivatives to second derivatives, thus penalizing only the latter ones and computing accurately the first ones which fits much more to fluid mechanics applications where gradients are

essentially important. The error functional with the second order regularization term reads as shown in Eq.(3).

$$E = \int_{\Omega} \left(\nabla I \cdot \mathbf{u} + I_t\right)^2 d\mathbf{x} + \int_{\Omega} \alpha^2 \cdot \left(|\nabla div\left(\mathbf{u}\right)|^2 + |\nabla curl\left(\mathbf{u}\right)|^2\right) d\mathbf{x}, \tag{3}$$

where $div\left(\mathbf{u}\right)$ is the divergence and $curl\left(\mathbf{u}\right)$ is the curl of the optical flow velocity vector. It can be seen in Eq.(3) that it is valid for arbitrary number of dimensions in this form.

When first- or second order regularization is used for making the OFC well posed, then the error functional E is minimized with the aid of the corresponding Euler-Lagrange equations. The Euler-Lagrange equations corresponding to the second order regularized error functional lead to a set of fourth order differential equations to be solved. The solution of these equations introduce severe numerical problems, so Corpetti *et al*. [7] has proposed to substitute the regularization term in Eq.(3) by the one shown in Eq.(4).

$$E = \int_{\Omega} \left(\nabla I \cdot \mathbf{u} + I_t\right)^2 d\mathbf{x} + \int_{\Omega} \alpha^2 \cdot \left(|div\left(\mathbf{u}\right) - \xi|^2 + \lambda|\nabla\xi|^2\right) d\mathbf{x} + \int_{\Omega} \alpha^2 \cdot \left(|curl\left(\mathbf{u}\right) - \zeta|^2 + \lambda|\nabla\zeta|^2\right) d\mathbf{x} \tag{4}$$

where ξ and ζ are auxiliary variables for which it is valid that during the iterative minimization of Eq.(4) $\xi \rightarrow div\left(\mathbf{u}\right)$ and $\zeta \rightarrow curl\left(\mathbf{u}\right)$, thus the regularization term in Eq.(4) transforms to be the same as in Eq.(3) when the iterations converged to the solution displacement field. Of course, additional Euler-Lagrange equations are needed for ξ and ζ that increases the computational cost but provides a stable numerical solution.

In all cases it has to be noted that due to its differential nature, the optical flow constraint can be applied only to a sequence of images which contain very small displacements of the objects. Theoretically the displacements should be infinitesimal, but practically it was found that displacements more than 2 pixels/voxels magnitude cannot be resolved accurately by this method. The optimal displacement value was found to be between 1 and 2 pixels/voxels based on preliminary investigations.

Originally, the optical flow was applied on 2-dimensional images and the first order regularization methods were used also in 3-dimensional volume-images. In this paper the authors show the extension of a 2nd order regularized optical flow method to 3-dimensional applications.

The paper is organized as follows: in section 2 the extension of the optical flow method, especially the 2nd order regularized functional to 3D is discussed, in section 3 details of the implementation of the algorithm are given, in section 4 results based on the use of synthetic images are shown and discussed, in section 5 the conclusions and perspectives are provided.

2. Extension of optical flow to three dimensions

The aim of this paper is the utilization of the well known optical flow method for detecting motion based on a sequence of three-dimensional images. The method of Lucas and Kanade [3], as well, as the method of Horn and Schunck [13] have already been extended to three dimensional case and are readily applicable [2].

2.1. First order regularization

The first order regularized functional has the form shown in Eq.(5) in 3D [2].

$$E = \int_{\Omega} \left(\nabla I \cdot \mathbf{u} + I_t\right)^2 d\mathbf{x} + \int_{\Omega} \alpha^2 \cdot \left(|\nabla u|^2 + |\nabla v|^2 + |\nabla w|^2\right) d\mathbf{x} \tag{5}$$

The first order regularized error functional leads to the set of Euler-Lagrange equations in 3D shown in Eq.(6).

$$\begin{aligned} I_x\left(I_x u + I_y v + I_z w + I_t\right) &= \alpha^2 \cdot \Delta u \\ I_y\left(I_x u + I_y v + I_z w + I_t\right) &= \alpha^2 \cdot \Delta v \\ I_z\left(I_x u + I_y v + I_z w + I_t\right) &= \alpha^2 \cdot \Delta w \end{aligned} \tag{6}$$

In Eq.(6) the subscripts indicate derivatives, f.e. $I_x = \partial I/\partial x$, t denotes time, Δ is the Laplace operator.

2.2. Second order regularization

For a second order regularized error functional, there is no readily available algorithm in three dimensions in the corresponding literature. The authors of this paper have taken the idea proposed by Corpetti *et al*. [7] as a basis due to its simplicity, robustness and reliability. Contrary to the algorithm used in [7] we have chosen a single resolution concept based on the application of the Euler-Lagrange equations to formulate the minimization problem and extended it to 3D. In this case the resulting equations had similar structure to those for the first order regularization

approach. The other difference with respect to the 2D formulation given in [7] is that in 3D, the auxiliary variable ζ becomes to be a vector $\zeta = [\zeta^x\ \zeta^y\ \zeta^z]$. The second order regularized functional has the form shown in Eq.(7).

$$\begin{aligned} E = \int_\Omega [(I_x u + I_y v + I_z w + I_t)^2 + \\ +\alpha^2 \cdot ((div\mathbf{u} - \xi)^2 + \lambda \left(|\nabla \xi|^2\right) + \\ + (curl\mathbf{u}|^x - \zeta^x)^2 + (curl\mathbf{u}|^y - \zeta^y)^2 + \\ + (curl\mathbf{u}|^z - \zeta^z)^2 + \\ \lambda \left(|\nabla \zeta^x|^2 + |\nabla \zeta^y|^2 + |\nabla \zeta^z|^2\right))] d\mathbf{x} \end{aligned} \tag{7}$$

In Eq.(7) superscipts x, y, z indicate the corresponding component of the vector quantities. The corresponding Euler-Lagrange equations are shown in Eq.(8). It can be seen that Eq.(6) and Eq.(8) are very similar in structure, they both have a Laplacian character. Theoretically the second order regularization does not include the Laplacian but the simplification proposed by Corpetti *et al*. [7] leads to the inheritance of this Laplacian character from the first order regularization method.

$$\begin{aligned} I_x \left(I_x u + I_y v + I_z w + I_t\right) = \alpha^2 \left(\Delta u + \left(\zeta_y^z - \zeta_z^y - \xi_x\right)\right) \\ I_y \left(I_x u + I_y v + I_z w + I_t\right) = \alpha^2 \left(\Delta v + \left(\zeta_z^x - \zeta_x^z - \xi_y\right)\right) \\ I_z \left(I_x u + I_y v + I_z w + I_t\right) = \alpha^2 \left(\Delta w + \left(\zeta_x^y - \zeta_y^x - \xi_z\right)\right) \end{aligned} \tag{8}$$

The additional terms that include purely the derivatives of the auxiliary variables have a strong influence on the equations that lead to a second order type regularization in the end of the computations. The Euler-Lagrange equations corresponding to the auxiliary variables are shown in Eq.(9).

$$\begin{aligned} -\left(u_x + v_y + w_z - \xi\right) = \lambda \cdot \Delta \xi \\ -\left(w_y - v_z - \zeta^x\right) = \lambda \cdot \Delta \zeta^x \\ -\left(u_z - w_x - \zeta^y\right) = \lambda \cdot \Delta \zeta^y \\ -\left(v_x - u_y - \zeta^z\right) = \lambda \cdot \Delta \zeta^z \end{aligned} \tag{9}$$

The Euler-Lagrange equations of the auxiliary variables also have a Laplacian character so this formulation of the second order regularization remains diffusive similarly to the first order regularization proposed by Horn and Shunck [13].

3. Implementation

3.1. Computing the derivatives and the Laplacian

It can be seen in the equations reported in this paper so far that derivatives of both the gray level field and the optical flow velocity field are needed. In case of second order regularization, there is also a need for computing the derivatives of the auxiliary variables. The variables can be sorted into two groups: the first group contains those variables which will be constant throughout the iterative solution of the optical flow equations; the other group contains those variables that change during the iterative solution. The gray levels I are contained by the first group as their differentiation has to be done only once, at the beginning of the process of optical flow solution. It also means that different differencing schemes can be applied for computing the image gray level derivatives than for the optical flow velocity derivatives. To obtain good quality derivatives of the gray levels, the best choice is the application of derivative filters [8],[15], [18] as these filters are robust against noise and provide a high order scheme.

The temporal derivative of the gray level field provided multiple possibilities to test: first, the four-point scheme proposed by Horn and Schunck [13] was modified to a nine-point scheme to provide symmetric information treatment around the current location.

The derivative filters are, however, not appropriate for discretizing a system of linear equations, thus for this purpose the central and fourth order schemes were used.

The Laplacian operator was approximated based on the proposal of Horn and Schunck [13], using $\Delta u \approx \kappa \left(\bar{u} - u\right)$, where u is the value of the variable at the current location, $\bar{u}$ is the average of the neighboring values. Here only the neighbor average has to be extended to 3D consequently, thus one can derive a 27-point scheme represented in Eq.(10).

$$\begin{aligned} \bar{u} = \tfrac{3}{44}\left(u_E + u_W + u_N + u_S + u_{RC} + u_{FC}\right) + \\ + \tfrac{3}{88}(u_{NE} + u_{NW} + u_{SE} + u_{SW} + u_{RN} + u_{RS} + \\ + u_{RE} + u_{RW} + u_{FN} + u_{FS} + u_{FE} + u_{FW}) + \\ + \tfrac{1}{44}(u_{RNW} + u_{RNE} + u_{RSW} + u_{RSE} + \\ + u_{FNW} + u_{FNE} + u_{FSW} + u_{FSE}), \end{aligned} \tag{10}$$

where the subscripts stand for directions from the current location as N-North, E-East, S-South, W-West, NE-North-East, NW-North-West, SE-South-East, SW-South-West, the subscript R stands for 'rear' (third coordinate is z_{i-1}), F stands for 'front' (third coordinate is z_{i+1}) slice, RC - rear center, FC - front center. Higher order approximations of the Laplacian were found to lead to the appearance of spurious oscillations in the velocity field, thus the authors decided to apply the second order accurate one that was described above.

3.2. Issues on geometric multigrid solver

The solution of the system of equations resulting from the regularized optical flow constraint is usually realized by means of an iterative method. The most frequently used tool for relaxing the equations is the Gauss-Seidel method, which is also the case in the present implementation. Analogously to the reasoning of Horn and Schunck [13], the main problem is the size of the images to be processed. The camera resolution recently is in the order of magnitude of 10^6 pixels, and in case of a volume image it is multiplied by the resolution in the third dimension that results in an order of magnitude of 10^9 voxels. This number of data would lead to a coefficient matrix of order of 10^{18} elements which is difficult to manage. For this reason the iteration stencils were implemented directly instead of applying a general matrix formulation. A detailed description of this technique is discussed in the basic paper of Horn and Schunck [13].

Since the equations have a Laplacian character, it was straightforward that a multigrid approach can be used to accelerate convergence. The multigrid method implemented in the present framework is a geometric multigrid based on the error correction scheme, about which detailed description can be found in [6]. Based on the idea of Horn and Schunck [13] one can evaluate the linear system of equations of the structure of $\mathbf{A}\mathbf{u} = \mathbf{b}$, with $\mathbf{A}$ coefficient matrix, $\mathbf{u}$ the unknown vector to be computed, $\mathbf{b}$ force vector, into a local formulation (located at position i, j, k) as shown in Eq.(11).

$$\mathbf{u}_{\mathrm{i,j,k}} + \mathbb{B}\overline{\mathbf{u}} = \mathbf{b}_{\mathrm{i,j,k}}, \tag{11}$$

where $\mathbb{B}\overline{\mathbf{u}}$ denotes all the operations which have to be carried out on the neighbour space of the location i, j, k. It can be seen that the local value of the unknown vector is separated explicitly from its neighbour space. The well known error correction scheme that is the basis for the multigrid method can be reformulated using the formulation in Eq.(11). Using $\mathbf{v}$ as the approximate solution, $\mathbf{u}$ as the exact solution of the equation and $\mathbf{r}$ as the residual of the equation one obtains Eq.(12) in the location i, j, k.

$$\mathbf{v}_{\mathrm{i,j,k}} + \mathbb{B}\overline{\mathbf{v}} = \mathbf{b}_{\mathrm{i,j,k}} + \mathbf{r}_{\mathrm{i,j,k}} \tag{12}$$

The error-correction equation can be obtained by subtracting Eq.(12) from Eq.(11) and by introducing the error vector itself as $\mathbf{e}_{i,j,k} = \mathbf{v}_{i,j,k} - \mathbf{u}_{i,j,k}$ one obtains Eq.(13).

$$\mathbf{e}_{i,j,k} + \mathbb{B}\overline{\mathbf{e}} = \mathbf{r}_{i,j,k}, \tag{13}$$

where, $\mathbf{e}_{i,j,k} = \left[e^u_{i,j,k}\ e^v_{i,j,k}\ e^w_{i,j,k}\right]$ denotes the local error vector and $\overline{\mathbf{e}} = [\overline{e^u}\ \overline{e^v}\ \overline{e^w}]$ is the neighbour average of the error vectors in the vicinity of the current location i, j, k. Eq.(13) is equivalent to the well known matrix form of $\mathbf{A}\mathbf{e} = \mathbf{r}$ as denoted in every textbook on numerical methods. For prolongation and restriction, the full weighted method was applied which were consistently extended to 3-dimensional space. The algorithm of the multigrid method is the same as reported in [6], thus it is not detailed here. The time for obtaining full convergence of the iterations is accelerated approximately by a factor of 5.

3.3. Parallelization concept with MPI

Due to the large size of the volume images it was needed to create a concept for a feasible treatment, so both the first order- and the second order regularization based solvers were parallelized. Parallel solution of systems of equations is already well established and it is mainly used to shorten the computational time. However it has not been used yet for optical flow problems, where more aspects arise. In the present case the main goal of parallelizing the optical flow solver was two fold: obviously the first aim was to accelerate the calculation, but the second, even the most important aspect was to provide appropriate environment for the treatment of large images. According to preliminary estimations, in case of an image of 1024^3 resolution with number type of 'double', the memory requirement of a second order regularized optical flow solution based on our three dimensional extension of the concept of Corpetti *et al.* [7] would be in the order of 100 GByte RAM, which is not suited for shared memory architectures. The code was parallelized on the way which is frequently applied for Laplacian type equations. The partitioning structure is represented in Figure.2.

The partitions are organized along one principle axis as shown in Figure.2a. This structure is valid also for the 3D case. The concept of the communication is outlined in Figure.2b. It can be seen that the partitions were divided into active and passive zones. The active zones participate and change their values during the computations, while the passive zones act as boundary conditions. The first and the last partition are bounded by boundary conditions on their 'free' sides. The computation procedure is as follows: after initialization each partition makes one single relaxation loop on the equations from the first element to the last element of their active zones. After each partition reached its end, the passive zones (or also called 'ghost layers') are updated by using the neighbour's first, or last corresponding active column. The next loop starts and uses the updated values in the ghost layers and the procedure is repeated until convergence is reached.

The multigrid solver necessitated further development of the parallelization, thus the restriction and prolongation, as well as the relaxation of the equations for the error-correction were parallelized using the same concept as discussed here above.

This structure of parallelization made it possible to use the units of a computational cluster as distributed memory stores. The parallelized version of the code thus starts with a

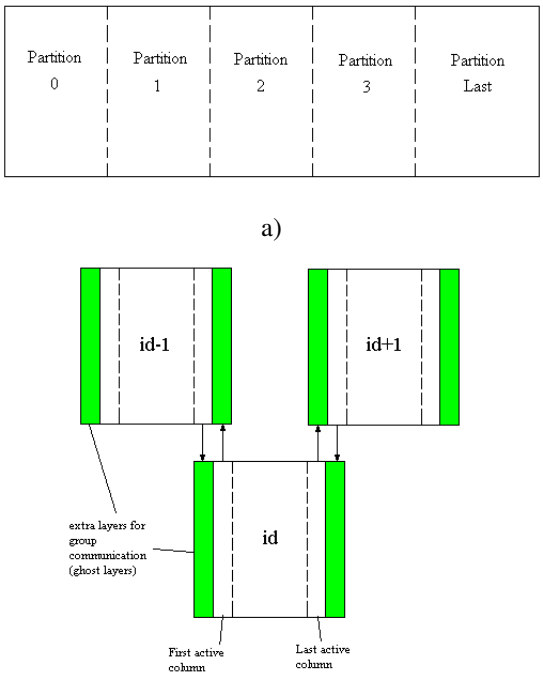

Figure 2. Partitioning concept for parallelization (a) and communication procedure (b)

distribution procedure, through which the large image is cut into small blocks and these blocks are sent to the individual units of the cluster. Each computational unit processes its own block and thus none of them has to treat an enormous amount of data. This way the maximum size of the image that can be treated, is exclusively limited by the size of the computational cluster. The results are then collected into a file that can be post-processed by an appropriate data visualizer software.

4. Results

4.1. Synthetic volume image generator

To avoid spurious effects originating from unexpected illumination-related noise sources that might influence the results, the algorithm was tested first on synthetic volume images. As the method discussed above is planned to be applied for the images originating from Particle Image Velocimetry, the synthetic images mimic the structure of these images. The observed volume is seeded by small particles which are supposed to follow the motion of the fluid. These particles usually appear on the images as light spots characterized by a Gaussian-like gray level distribution. In 3D the particles appear as spheres with varying gray level along their radius. A typical volume image and a slice along its center is shown in Figure.3.

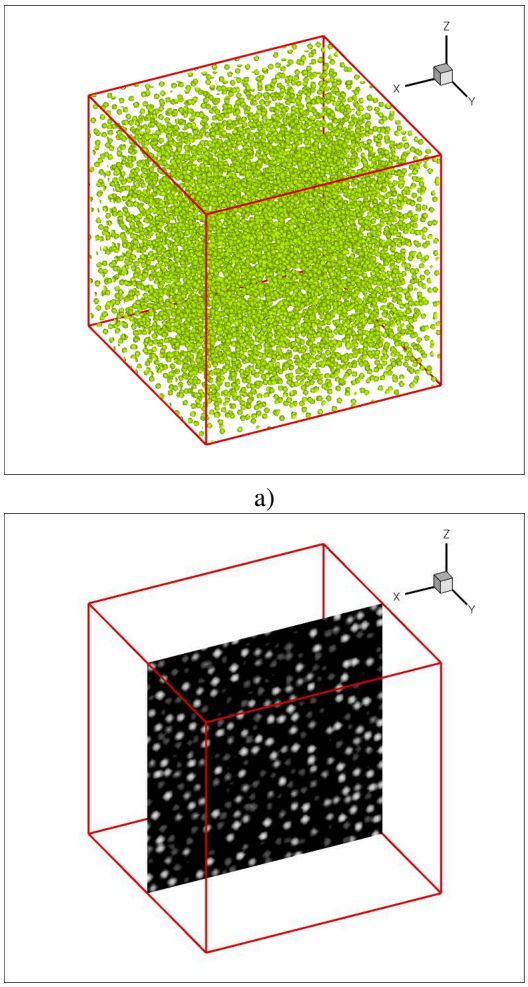

Figure 3. A typical volume image with the particles indicated by spheres (a) and a slice of the volume indicating the gray level distribution (b)

The motion was imitated by displacing the position of the particles with a known displacement vector field. Although several motion patterns were investigated during the validation period of the optical flow software, here only the so called Hill's spherical vortex is presented due to the limited space of this paper. Indeed Hill's vortex was found to be a good representative of most of the critical motion features that are expected to occur for fluid mechanics applications.

4.2. Hill's spherical vortex

The pattern of this motion is a vortex which is located inside a sphere of radius R. The motion is axisymmetric with an arbitrarily oriented axis. Let x denote the distance along the axis, d the distance normal to the axis and U the velocity in the free stream, far away from the vortex. In this case the field of motion can be described by two Stokes stream functions, out of which, one describes the velocity field in-

side the sphere, the other describes that of the exterior field [14]. The two stream functions are represented in Eq.(14).

$$\psi_{interior} = \frac{3}{4}U \cdot d^2 \left(1 - \frac{d^2+x^2}{R^2}\right)$$
$$\psi_{exterior} = -\frac{1}{2}U \cdot d^2 \left(1 - \frac{R^3}{(x^2+d^2)^{3/2}}\right) \quad (14)$$

The axial and the radial components of the velocity vector can be obtained by differentiating the Stokes stream function. The axial component of the velocity is $u_{ax} = (1/d)\,\partial\psi/\partial x$, and the radial component of the velocity is $u_{rad} = -(1/d)\,\partial\psi/\partial d$. The axial and radial components of the velocity vector were transformed into a general Descartes coordinate system with orthogonal axes x, y, z.

4.3. Velocity field obtained by using second order regularized optical flow constraint

The exact field and the optical flow solution can be seen in Figure.4. The flow field is represented by means of streamlines and a contour plot in the y-normal central plane. The axis of the flow is now oriented towards the positive x-direction. The radius of the vortex is 25 voxels, the size of the domain is 100^3 voxels, the free stream velocity is 1.5 voxels/frame. The derivatives of the gray level fields were computed by the Deriche derivative filter [9], the temporal derivative was computed with a 9-point single slice scheme. The velocity derivatives were approximated by a fourth order scheme. It can be seen that there is a good agreement between the exact and the optical flow solution. The major visible difference is the shape of the streamlines inside the vortex. The exact solution shows that the streamlines are closed curves, while the optical flow solution resembles a spiralling trajectory. This error is due to the relatively low resolution of the motion by means of particles. It can be seen in Figure.3b, that in the region of the vortex there are only few particles that cannot provide an exact pattern. Increasing the resolution improves the shape of streamlines here. The difference in the magnitude of velocity vectors between the two fields related to the exact solution is shown in percentage in Figure.5. One can observe that in the majority of the domain the difference is below 10% of the exact solution. Higher errors can be seen in the region of high velocity gradients, i.e. in the vortex core and in the stagnation points.

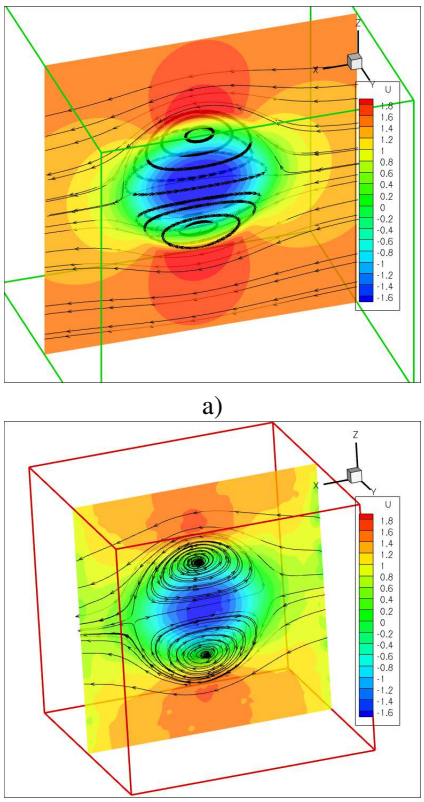

Figure 4. Velocity field of Hill's vortex (a) and the solution of a second order regularized optical flow (b). Contours represent the velocity component in the axial direction

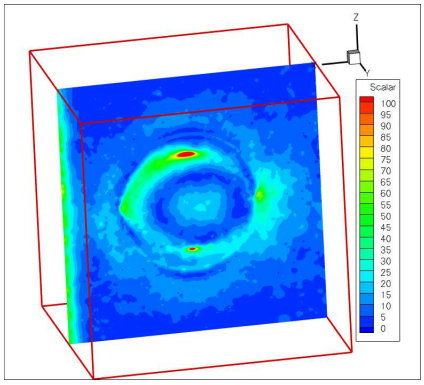

Figure 5. Difference magnitude field between the exact and optical flow solution represented in percentages related to the exact solution

5. Conclusions

In this paper a concept of the extension of the well known optical flow method from 2D images to 3D volume images was discussed. The extension of the Lucas and Kanade method and the method of Horn and Schunck has been previously done and available in the corresponding literature, but for the second order regularized optical flow constraint there was no information for 3D applications. The second order regularization, presented here in detail, was based on the idea of Corpetti *et al.* [7] but by using different minimization concept. This concept provided the possibility for the extension of this formulation to 3D. Due to the

large size of the volume images the numerical implementation of the solution of the corresponding equations was based on locally evaluated stencil formulation and not in the more general matrix form. To accelerate convergence, the error-correction based geometric multigrid method was implemented. To accelerate the iterative Gauss-Seidel relaxation of the equations, as well, as for providing a flexible distributed memory structure, the program was parallelized by means of MPI. The distributed memory architecture provides a good basis for treating images that are characterized by a size that can not be stored in a single, shared memory structured computer. The performance of the second order regularized optical flow method was demonstrated by means of a synthetic volume image containing particles. The particles were displaced by a known vector field which was the velocity field of the axisymmetric Hill's vortex. The optical flow solution showed a good agreement with the exact solution.

It was discussed that the optical flow method is restricted only to small displacements, whereas in case of the flow of a fluid several different displacements can occur. To overcome this problem the correlation method is planned to be used to determine a coarse vector field for the large displacements, and an interpolation will be applied to generate the fine resolved vector field. The images will then be modified by using the interpolated vector field to remove the large displacements and thus to enable the optimal conditions for the optical flow solver. This way the optical flow method can complement the correlation method by increasing the resolution of the results as well, as their accuracy. It has been mentioned that the optical flow constraint can be solved within acceptable accuracy only if the displacements are 'infinitesimal', practically smaller than 2 pixels/voxels. Similarly to the 2D solution proposed in the work of Heitz *et al*. [12] the authors of this paper will use the cross correlation method to determine the flow field with large displacements. Concerning validation on real data, experiments are being carried out at the moment.

Acknowledgments

The authors gratefully acknowledge the French National Research Agency for financing this project (VIVE3D).

References

[1] R. Adrian. Twenty years of particle image velocimetry. *Experiments in Fluids*, 39(2):159–169, 2005. 1, 2

[2] J. Barron and N. Thacker. *Tutorial: Computing 2D and 3D optical flow*. Tina Memo No. 2004-012, Internal document of Imaging Science and Biomedical Engineering Division, Medical School, University of Manchester, 2004. 3

[3] S. Beauchemin and J. Barron. The computation of optical-flow. *Surveys*, 27(3):433–467, September 1995. 2, 3

[4] D. Béréziat and I. Herlin. *Solving ill-posed image processing problems using data assimilation. Application to optical flow*. INRIA Research report, RR-6477, 2008. 2

[5] M. Black and P. Anandan. The robust estimation of multiple motions: Parametric and piecewise-smooth flow fields. *Computer Vision and Image Understanding*, 63(1):75–104, January 1996. 2

[6] W. Briggs, V. Henson, and S. McCormick. *A Multigrid Tutorial*. Second etition, Society for Indurstrial and Applied Mathematics, 2000. 5

[7] T. Corpetti, D. Heitz, G. Arroyo, E. Mémin, and A. Santa-Cruz. Fluid experimental flow estimation based on an optical flow scheme. *Experiments in Fluids*, 40:80–97, 2006. 2, 3, 4, 5, 7

[8] R. Deriche. Recursively Implementing the Gaussian and Its Derivatives. In *Proc. Second International Conference On Image Processing*, pages 263–267, Singapore, Sept. 7-11 1992. 4

[9] R. Deriche. *Recursively implementing the Gaussian and its derivatives*. INRIA Sophia-Antipolis, Rapports de Recherche, Programme 4, Robotique, Image et Vision, No.1893, Avril, 1993. 7

[10] G. E. Elsinga, F. Scarano, B. Wieneke, and B. W. van Oudheusden. Tomographic particle image velocimetry. *Experiments in Fluids*, 41(6):933–947, December 2006. 1

[11] A. Fincham. 3 component, volumetric, time-resolved scanning correlation imaging velocimetry. In *5th International Symposium on Particle Image Velocimetry*, pages 1–10, September 2003. 1

[12] D. Heitz, P. Héas, E. Mémin, and J. Carlier. Dynamic consistent correlation-variational approach for robust optical flow estimation. *Experiments in Fluids*, 45:595–608, 2008. 8

[13] B. Horn and B. Schunck. Determining optical flow. *Artificial Intelligence*, 17:185–203, August 1981. Article de référence. 2, 3, 4, 5

[14] H. Moffatt. Generalised vortex rings with and without swirl. *Fluid Dynamics Research*, 3:22–30, 1988. 7

[15] O. Monga, R. Deriche, and J. Rocchisani. 3D edge detection using recursive filtering: application to scanner images. *CVGIP: Image Understanding*, 53(1):76–87, 1991. 4

[16] N. Papadakis and E. Mémin. Variational assimilation of fluid motion from image sequence. In *SIIMS'08*, volume 1, pages 343–363, 2008. 2

[17] P. Ruhnau and C. Schnorr. Optical stokes flow estimation: an imaging-based control approach. *Experiments in Fluids*, 42:61–78, 2007. 2

[18] E. Simoncelli. Design of multi-dimensional derivative filters. In *First IEEE International Conference on Image Processing, Austin, Texas*, pages 790–793, 1994. 4

[19] D. Suter. Motion estimation and vector splines. In *Conference on Computer Vision and Pattern Recognition*, pages 939–942, 1994. 2